ROYAL SOCIETY
OF CHEMISTRY

REVIEW

Check for updates

Decoding the tactics for coacervate pedestrian crossing the phospholipid membrane

Huimin Yang,[ab] Minghao Wei[ab] and Yan Qiao [ID] *[ab]

Coacervate microdroplets based on liquid–liquid phase separation (LLPS) have emerged as versatile models for protocells, membraneless organelles and smart drug delivery carriers. Understanding the mechanisms of coacervates crossing lipid membranes is of great significance in synthetic cell engineering, cell physiology analysis, and transmembrane drug delivery. In this review, we systematically summarize the mechanisms by which coacervates cross phospholipid bilayers of liposomes or cells, which are classified based on whether membrane-remodelling processes are present. Two major mechanisms are introduced, including vesicular engulfment driven by electrostatic interaction, photoswitchable phospholipids, caveolin and actin polymerization, and direct penetration mediated by lipid rafts and phospholipid defects. These findings deepen the understanding of mass and signal exchange across cellular boundaries and underscore the potential applications of coacervates for sophisticated synthetic cells, biosensors and drug delivery systems.

1. Introduction

From primitive protocells to modern eukaryotic cells, biological membranes serve as essential barriers to distinguish self and non-self, subcompartments,[1] enabling vital functions such as selective mass,[2–4] signal[5–7] and energy transport.[8,9] Among these functions, mass transport is indispensable for maintaining cellular functions, particularly for small molecules (*e.g.*, ions,[10,11] amino acids,[12] and nucleotides),[13] macromolecules (*e.g.*, proteins,[14,15] nucleic acids[16] and polysaccharides),[17] and nano- to micro-scale particles (*e.g.*, exosomes,[18] apoptotic bodies,[19] and extracellular matrix particles).[20] Previous studies and reviews have elucidated the transmembrane mechanisms for these species including passive diffusion, transporter-mediated entry, and other methods of cytosolic entry such as clathrin-mediated endocytosis,[21] caveolin-mediated endocytosis,[22] and macropinocytosis.[23,24] Nevertheless, the mechanisms governing the translocation of microscale coacervates with liquid nature across phospholipid membranes remain rarely summarized.[25]

Coacervate microdroplets formed through liquid–liquid phase separation (LLPS) have emerged as versatile models in both life and materials sciences[26,27] due to their dynamic structure, selective molecular sequestration and molecularly crowded interior.[28–31] In the past few decades, they have been widely studied as protocells that exhibit cell-like behaviours, such as compartmentalization,[32–34] molecular enrichment,[35,36]

enzymatic reaction enhancement,[37–41] communication,[42–47] predation,[48] and phagocytosis.[49] Concurrently, coacervates underwent deformation, fusion, rapid molecular exchange,[47] and reversible assembly/disassembly, making them ideal models for membraneless organelles (MLOs) associated with transcription regulation,[50] RNA processing and transport,[51,52] DNA damage repair,[53] stress response,[54] innate immunity,[55] and neurotransmitter release.[56] Besides, owing to superior encapsulation efficiency, high programmable design and efficient cellular internalization, coacervates are also programmable, responsive scaffolds for designing adaptive soft materials,[57–59] catalytic microreactors,[39,60] and drug delivery carriers[61–64] particularly for macromolecular therapeutics (proteins,[65] nucleic acids[66,67] and polysaccharides[68]). The studies about coacervate–phospholipid membrane interactions provide critical insights for the rational design of sophisticated synthetic cells, advanced biosensors, and smart drug delivery systems.

Herein, this review summarizes recent advances in the transmembrane mechanisms of coacervates into liposomes or cells, focusing on vesicular engulfment and direct penetration based on whether transport vesicles are formed. According to distinct physicochemical or cellular factors, we refine the two mechanisms into six pathways including electrostatic interaction-, photoswitchable phospholipid-, caveolin-, and actin polymerization-driven vesicular engulfment, and lipid raft- and phospholipid defect-mediated direct penetration. By systematically analysing the driving factors, membrane-remodelling processes, and corresponding cellular entry pathways, this review is expected to advance the mechanistic understanding of cell complexity, inform the rational design of functional synthetic cells, and develop new drug delivery systems.

[a]Beijing National Laboratory for Molecular Sciences (BNLMS), Laboratory of Polymer Physics and Chemistry, CAS Research/Education Center for Excellence in Molecular Sciences, Institute of Chemistry, Chinese Academy of Sciences, Beijing 100190, China. E-mail: yanqiao@iccas.ac.cn

[b]University of Chinese Academy of Sciences, Beijing 100049, China

2. Mechanisms of coacervate droplets crossing phospholipid membranes

Coacervate–liposome interactions involving a coacervate (α), a liposome (β) and an aqueous phase (γ) exhibit rich interfacial behaviours governed by the balance between adhesive (coacervate–membrane interactions) and cohesive forces (intra-coacervate interactions).[69] This balance defines three distinct wetting states: non-wetting (detachment), partial wetting (limited adhesion and spreading) and complete wetting (extensive contact and membrane envelopment). Transitions between these states are quantitatively described by the contact angles (θ_α, θ_β, and θ_γ) between the interfaces at the three-phase contact line, serving as key physical parameters that reflect the thermodynamic equilibrium at the three-phase boundary.[70] Varying adhesion intensities lead to non-wetting ($\theta_\alpha = \theta_\beta = 180°$), partial wetting ($0° < \theta_\alpha < 180°$ and $0° < \theta_\beta < 180°$), or complete wetting ($\theta_\alpha = 180°$ and $\theta_\beta = 0°$) behaviours. Among these, partial wetting represents the most complicated state, as illustrated in Fig. 1a. A contact angle $\theta_\beta < 90°$ typically indicates

favourable wetting, whereas $\theta_\beta > 90°$ indicates poor wetting. Notably, a decrease in θ_β correlates with increased membrane engagement, with a value approaching 0° indicating the onset of complete membrane engulfment. This fundamental understanding of wetting behaviour provides a critical physical framework for analysing subsequent transmembrane events.

Recent advances in molecular dynamics simulations have significantly enhanced the understanding of coacervate–phospholipid membrane complex interactions,[71–73] particularly in the context of membrane engulfment and curvature sensing. Ghosh and Lipowsky et al. investigated the engulfment of LLPS-induced droplets by lipid bilayer nanovesicles using dissipative particle dynamics (DPD) simulations.[74] Droplet size was identified as a decisive factor in determining the extent of engulfment by nanovesicles (Fig. 1b). This process was found to be strictly constrained by the geometric relationship between the available membrane area of the vesicle and the volume of the droplet. The isoperimetric inequality dictated a critical droplet volume that could be fully enclosed by the limited membrane area. For smaller droplets ($D_{droplet} = 11.2$ nm) whose volume was below this critical threshold, the vesicle membrane had sufficient area to achieve complete engulfment, resulting in
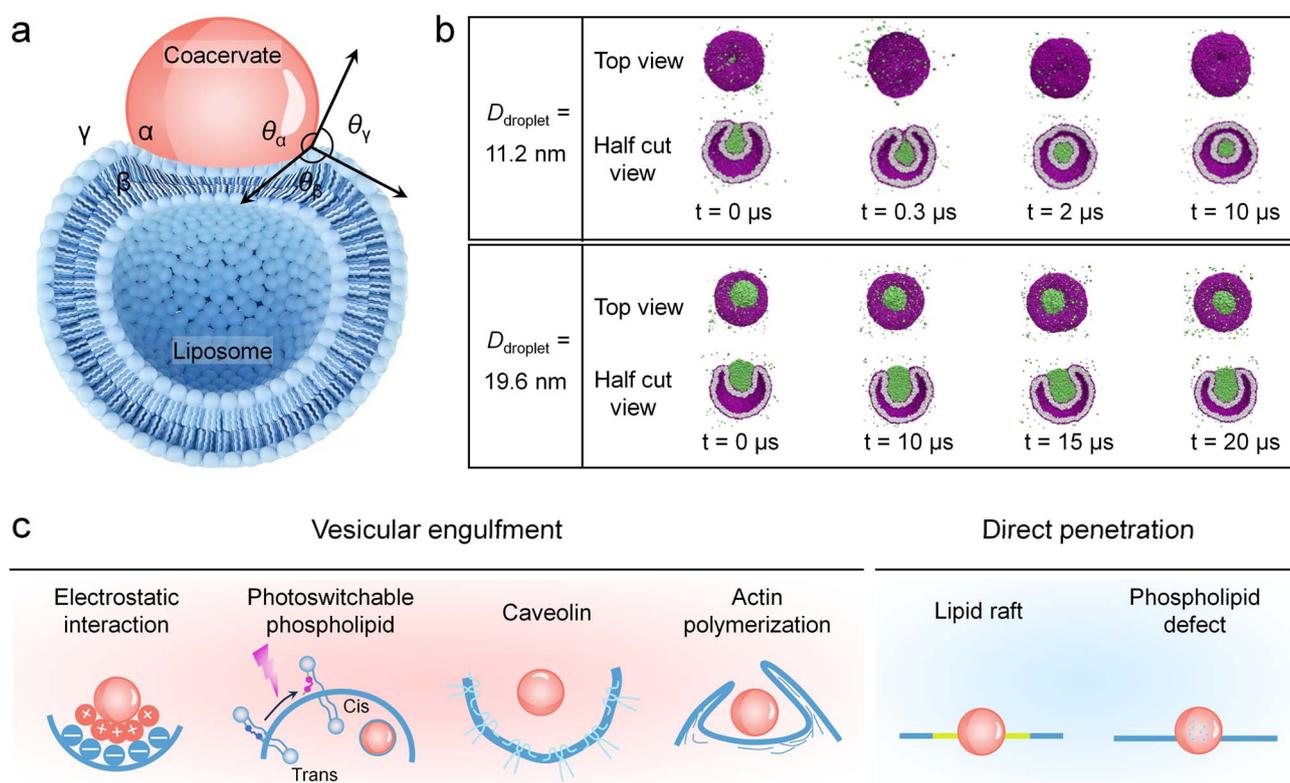

Fig. 1 Illustrations and mechanisms of coacervates crossing phospholipid membranes. (a) Schematic diagram of a contacting coacervate–liposome system involving a coacervate (α, red), a liposome (β, blue) and an aqueous phase (γ) along with three contact angles (θ_α, θ_β, and θ_γ). (b) Molecular dynamics simulations revealed that the coacervate droplet size influenced the engulfment efficiency of liposomes. Complete engulfment with a closed membrane neck was observed for the smaller droplet ($D_{droplet} = 11.2$ nm), whereas partial engulfment with an open membrane neck was observed for the larger droplet ($D_{droplet} = 19.6$ nm). (c) Schematic classifications of two major transmembrane mechanisms of coacervates, including vesicular engulfment (e.g., driven by electrostatic interaction, photoswitchable phospholipids, caveolin, or actin polymerization) and direct penetration (e.g., driven by lipid rafts or phospholipid defects). (b) Reproduced with permission from ref. 74. Copyright (2023) Springer Nature.

a closed membrane neck that subsequently underwent fission to form a nested daughter vesicle. In contrast, for larger droplets ($D_{droplet}$ = 19.6 nm) whose volume exceeded the membrane's encapsulation capacity, the process was limited to partial engulfment with the membrane neck remaining open. Thus, the final engulfment outcome was fundamentally determined by the competition between droplet volume and available vesicle membrane area, highlighting the essential role of physical geometric constraints in cellular processes.

Beyond these geometric constraints, a major distinction at the cellular level lies in the reliance on specific receptor mediation, which categorizes uptake mechanisms into classical and non-classical pathways. Classical endocytosis refers to the canonical, receptor-triggered cellular uptake pathways mediated by clathrin, a highly regulated process involving precise molecular recognition, coat assembly, and protein-driven membrane fission.[75,76] In contrast, non-classical endocytosis includes multiple pathways that operate independently of the clathrin machinery. These include physicochemical-driven membrane engulfment, caveolin- or actin polymerization-mediated endocytosis,[77] lipid raft-dependent internalization and phospholipid defect-mediated direct penetration.

Current advances in coacervate internalization consistently demonstrate that their entry into cells or membrane-enclosed compartments occurs primarily *via* the non-classical pathways, bypassing the classical endocytosis to enable efficient cellular uptake and cargo delivery. This review summarizes recent advances in the transmembrane mechanisms of coacervates, focusing on vesicular engulfment (*e.g.*, driven by electrostatic interaction, photoswitchable phospholipids, caveolin and actin polymerization) and direct penetration (*e.g.*, driven by lipid rafts and phospholipid defects) (Fig. 1c).

3. Coacervates crossing phospholipid membranes by the vesicular engulfment mechanism

Vesicular engulfment represents a fundamental transmembrane mechanism for coacervate internalization, involving the progressive wrapping of the coacervates by the lipid bilayers and substantial membrane deformation, culminating in the formation of membrane-bound transport vesicles. This mechanism is driven by distinct physicochemical or biologically active factors, including electrostatic interaction, photoswitchable phospholipids, caveolin, actin polymerization, *etc.* The following sections detail these key pathways of vesicular engulfment and their roles in facilitating efficient cargo entry while preserving membrane integrity.

3.1 Engulfment mediated by electrostatic interaction

When coacervates and liposomes are oppositely charged, electrostatic interaction plays a central role in mediating their interfacial behaviour, driving a progression from contact to partial wetting and eventual engulfment (Fig. 2a).[78] The strength of the electrostatic interaction determines the final wetting state. Under a weak electrostatic interaction,

coacervates and liposomes exhibit only adhesion and favourable partial wetting (Fig. 2b). Engulfment occurs exclusively when the interaction exceeded a specific threshold. Further increases in electrostatic interaction strength led to poor partial wetting and complete wetting (Fig. 2b).

As demonstrated by Lu and Spruijt *et al.*, a representative system consisted of negatively charged spermine/polyuridylic acid (polyU) coacervates and positively charged 1-palmitoyl-2-oleoyl-*sn*-glycero-3-phosphorylcholine (POPC)/1,2-dioleoyl-3-trimethylammoniumpropane (DOTAP)/cholesterol liposomes (Fig. 2c).[78] The surface charges of coacervates and liposomes were regulated by the ratio of spermine/polyU and the mass fraction of DOTAP, respectively. By lowering the spermine-to-polyU ratio (from 105 : 1 to 2 : 1), the negative charges of spermine/polyU droplets were progressively increased, resulting in a progression from favourable partial wetting (105 : 1) to engulfment (52 : 1, 7 : 1), followed by unfavourable wetting (3 : 1) and complete wetting (2 : 1) (Fig. 2d) upon interaction with positively charged liposomes (20 wt% DOTAP). Alternatively, by increasing the DOTAP content (from 0 wt% to 35 wt%), the positive charges were systematically enhanced, yielding a sequence of wetting states involving non-wetting (0 wt%), favourable partial wetting (10 wt%), engulfment (20 wt%), unfavourable partial wetting (30 wt%), and complete wetting (35 wt%) (Fig. 2e) upon interaction with spermine/polyU coacervates (13 : 1). Similarly, positively charged coacervates (*e.g.*, poly-L-arginine trifluoroacetic acid (R_{10})/polyU, poly(-diallyldimethylammonium chloride) (PDDA)/adenosine 5′-triphosphate disodium salt hydrate (ATP), GFP-K_{72}/RNA coacervates) were able to be engulfed by negatively charged 1-palmitoyl-2-oleoyl-*sn*-glycero-3-phospho-(1′-*rac*-glycerol) (POPG)-containing liposomes. Beyond varying compositions of aggregates, electrostatic interaction is also modulated by the salt shielding effect and the degree of protonation, offering ways to fine-tune the wetting dynamics and engulfment outcomes.[79]

The electrostatically driven engulfment provides an efficient pathway for biomolecular delivery into cells. Armstrong and Perriman *et al.* positioned coacervates onto specific regions of the stem cell membrane using optical tweezers guided by a dynamic holographic assembly device.[80] The electrostatic interactions between the positively charged coacervates and the negatively charged cell membranes promoted spontaneous fusion, enabling effective transfer of biomolecules (*e.g.*, eGFP, ssDNA, and Hoechst) without compromising cell viability or differentiation capacity. Among these, macromolecules that could not passively cross the plasma membrane, such as eGFP and ssDNA, gained access to the cell interior through endocytosis after being encapsulated within coacervates. Although the electrostatically mediated transmembrane is straightforward and efficient, it lacks interaction specificity for particular cellular targets.

3.2 Engulfment mediated by photoswitchable phospholipids

The responsiveness of biological membranes to external stimuli represents a key property that enables active regulation of their
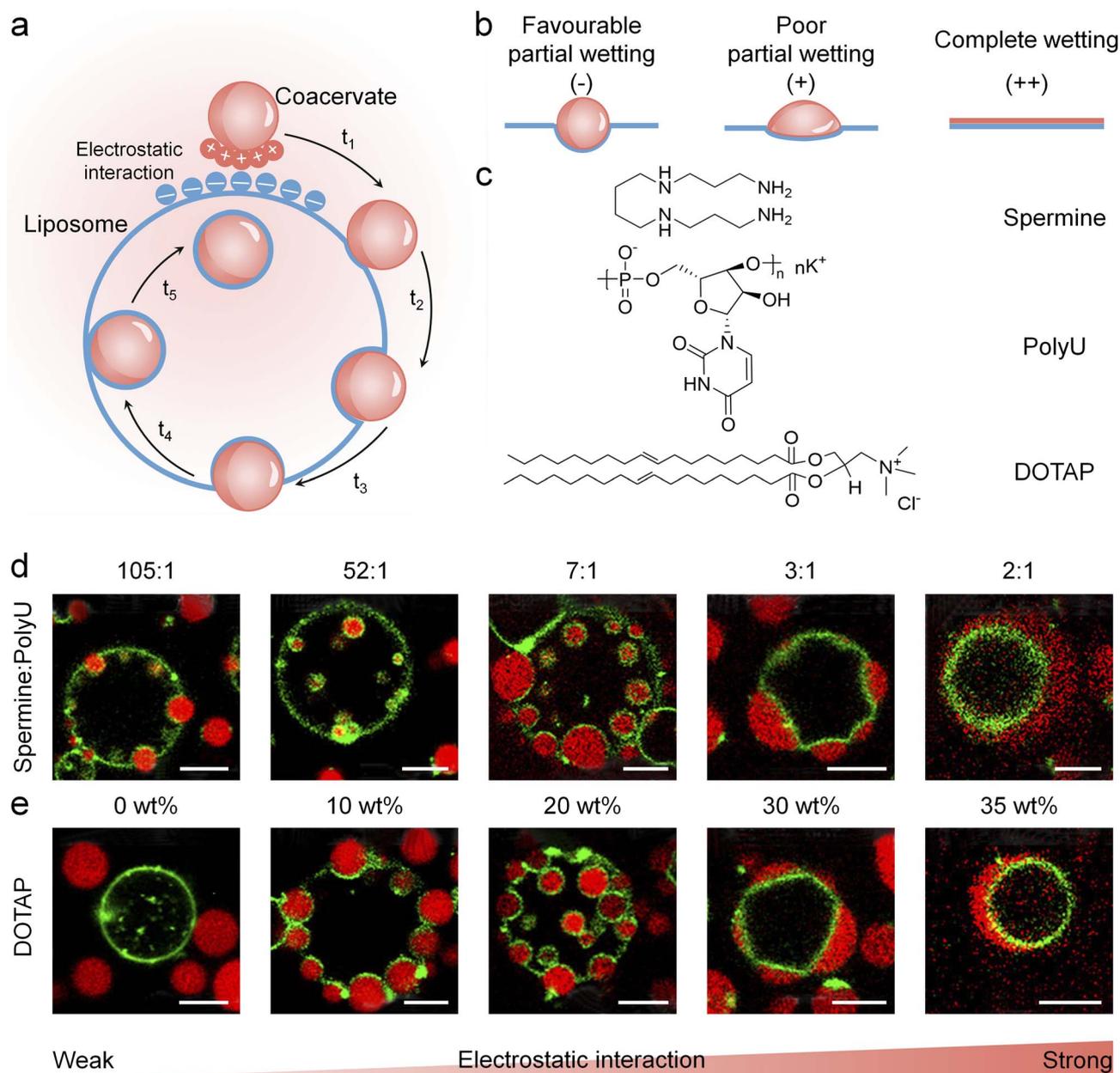
Fig. 2 Electrostatic interaction-mediated engulfment of coacervates by liposomes. (a) Schematic diagram of electrostatic attraction-driven coacervate engulfment, illustrating the sequential process (t_1–t_5) of the coacervate, including contacting, partial wetting, and complete engulfment. (b) Schematic diagrams depicting favourable partial wetting, poor partial wetting and complete wetting of coacervates on liposome membranes, where weak electrostatic interactions (−) led to favourable partial wetting, strong interactions (+) resulted in poor partial wetting, and excessively strong interactions (++) resulted in complete wetting. (c) Chemical structures of spermine, polyU, and DOTAP. The spermine/polyU ratio tuned the negative surface charges of coacervates, while the DOTAP mass fraction regulated the positive surface charges of POPC/cholesterol liposomes. (d and e) Fluorescence microscopy images presenting that the engulfment degree was tuned by the surface charges of either coacervates (d) or liposomes (e). Enhanced electrostatic interaction promoted the continuous transition from non-wetting to complete wetting. Scale bars, 5 μm. Reproduced with permission from ref. 78. Copyright (2022) American Chemical Society.

interactions with coacervates. Variations in temperature,[81] electric fields,[82–84] or pH gradients modulate the membrane area-to-volume ratio or the electrostatic landscape,[85] leading to budding, tubulation, or invagination. Furthermore, locally applied mechanical or chemical forces drive deformation *via* membrane tension gradients or curvature-inducing molecules.[86,87] Among these stimuli, light stands out due to its high

spatiotemporal precision, minimal invasiveness, and biocompatibility, making it an excellent tool for programmable membrane processes.[88]

Integrating photoresponsive molecules into phospholipid membranes provided a possible pathway to achieving such modulation, enabling photo-triggered engulfment of coacervates by regulating coacervate–membrane interactions.
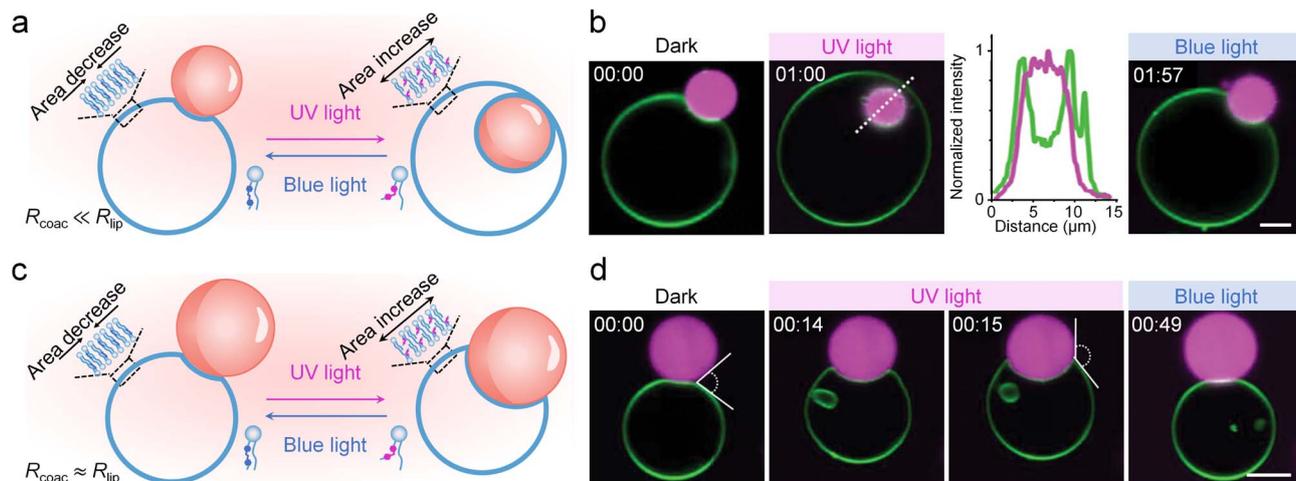
Fig. 3 Photoswitchable phospholipid-mediated coacervate engulfment by phospholipid membranes. (a) Schematic of complete engulfment of a smaller coacervate by a photoswitchable liposome. UV-induced *trans*-to-*cis* photoisomerization of azobenzene phospholipids increased the membrane area and triggered engulfment, while blue light reversed this process *via* *cis*-to-*trans* back-isomerization. (b) Fluorescence microscopy images and corresponding intensity profiles (along the white dashed line) presenting the reversible photoswitchable engulfment and release of the coacervate (magenta) by the liposome (green). (c) Schematic of partial engulfment for a coacervate of comparable size, with blue light mediating process reversal. (d) Fluorescence microscopy images presenting the partial engulfment and reversible release of the coacervate (magenta) by the liposome (green). (b and d) Scale bars, 5 μm. Reproduced with permission from ref. 89. Copyright (2024) Wiley-VCH.

Mangiarotti and Dimova *et al.* designed giant unilamellar vesicles (GUVs) containing photoswitchable azobenzene phospholipid analogs (azo-PC), enabling precise photoswitchable regulation over glycinin coacervate engulfment.[89] Upon UV irradiation, azo-PC underwent *trans*-to-*cis* photoisomerization, rapidly increasing the membrane area by approximately 18%. This excess membrane area enhanced the adhesion interface to coacervates, thereby promoting their engulfment. The extent of coacervate internalization exhibited a distinct size-dependence, governed by the geometric relationship between vesicles and coacervates. When coacervates were significantly smaller than vesicles, the newly generated membrane area was sufficient to achieve complete wrapping and endocytosis, forming a closed membrane neck (Fig. 3a and b). In contrast, for coacervates comparable in size to vesicles, the same area expansion primarily enlarged the adhesive interface, resulting in partial wetting without full internalization (Fig. 3c and d). This behaviour was energetically determined, as maximizing the coacervate–membrane contact minimized the free energy of the system more efficiently than storing excess area in membrane nanotubes. The entire process was fully reversed by blue light, which triggered *cis*-to-*trans* back-isomerization, reducing the membrane area and releasing coacervates. This pathway provided exceptional spatiotemporal precision and reversibility, establishing a versatile platform for the design of synthetic cellular compartments and on-demand drug-delivery systems.

3.3 Endocytosis mediated by caveolin

Endocytosis serves as a principal process for cellular uptake of macromolecules and specific species. In mammalian cells, endocytosis includes the caveolin-mediated pathway, a well-characterized form of clathrin-independent endocytosis that relies on the assembly of caveolar structures and caveolin proteins at the plasma membrane.[90] Studies focusing on coacervate translocation across phospholipid membranes also confirmed that caveolin-mediated endocytosis constitutes a key pathway for the efficient cellular internalization of coacervates.

Within the broad context of elucidating cellular uptake pathways for biomolecular condensates, Halder and Jokerst *et al.* offered an instructive example of pathway-specific internalization.[91] They demonstrated that complex coacervates formed between an anionic D_{10} peptide and a cationic peptide containing a β-sheet-promoting FFVLK sequence and a PyTPE aggregation-induced emission (AIE) luminogen (PyTPE-FFVLKR_{10}) were efficiently internalized by murine colon adenocarcinoma (MC38) cells experiencing early endosome trafficking and subsequent endosomal escape (Fig. 4a). In the cell culture environment, the physicochemical properties of these coacervates underwent changes. After 1 h of exposure to culture medium containing 10% fetal bovine serum (FBS), the average coacervate size decreased from 570 nm to 310 nm, accompanied by a shift in zeta potential from −12.17 mV to −17.29 mV. To delineate the entry pathway, a systematic pharmacological inhibition study was conducted, coupled with quantitative flow cytometry (Fig. 4b) and qualitative confocal microscopy (Fig. 4c). The results revealed a significant suppression of coacervate uptake upon treatment with filipin, a specific inhibitor of caveolin-mediated endocytosis. In contrast, inhibitors targeting clathrin-mediated endocytosis (chlorpromazine, CPZ), cholesterol-disrupting agents (methyl-β-cyclodextrin, MβCD), and macropinocytosis inhibitor (ethylisopropylamiloride, EIPA) exhibited minimal effect. The energy-dependent nature of the process was further confirmed by a near-complete inhibition of uptake at 4 °C. The study therefore concluded that caveolin-mediated endocytosis
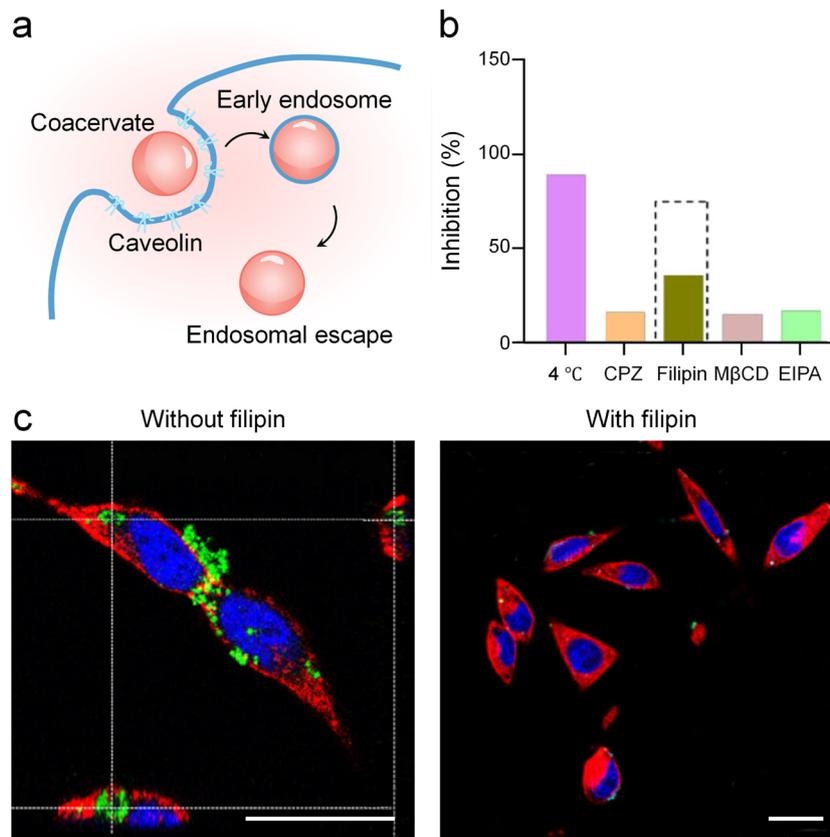
Fig. 4 Caveolin-mediated coacervate endocytosis by a phospholipid membrane. (a) Schematic of caveolin-mediated endocytosis of coacervates in a phospholipid membrane, including early endosome trafficking and subsequent endosomal escape. (b) Flow cytometry-derived inhibition rate columns showing the inhibition of coacervate uptake by various endocytic inhibitors. The dashed box highlights that filipin caused a significant suppression of uptake, suggesting that caveolin-mediated endocytosis served as the primary pathway, whereas CPZ, MβCD, and EIPA showed minimal effects. Moreover, near-complete inhibition observed at 4 °C confirmed that the internalization process was energy-dependent. (c) Confocal microscopy images showing the inhibition of coacervate internalization upon treatment with the caveolin inhibitor filipin. Scale bars, 25 μm. (b and c) Reproduced with permission from ref. 91. Copyright (2025) American Chemical Society.

represented the primary pathway of cellular entry for these β-sheet-stabilized, AIE-active peptide coacervates. This result provided valuable molecular-level understanding for the rational design of advanced coacervate-based delivery systems with tailored cellular entry pathways.

3.4 Endocytosis mediated by actin polymerization

While the involvement of caveolin provides a well-defined pathway for the cellular entry of coacervates, evidence points to the existence of alternative yet equally crucial internalization pathways. This section explores actin polymerization-driven endocytosis, particularly macropinocytosis.

Actin polymerization is essential for driving cell membrane endocytosis by generating force[92] and shaping membrane curvature.[93,94] Iwata and Futaki et al. described a pathway for the intracellular delivery of immunoglobulin G (IgG) and other macromolecules using coacervates formed by the interaction of IgG with a cationic amphiphilic peptide (Fig. 5a).[95] The process involved coacervates (2 μm in size) settling (20 min) and attaching (24 min) to the cell surface, which triggered local actin polymerization and membrane ruffling, thereby leading to

coacervate internalization (25 min 20 s). Time-lapse imaging further confirmed that following attachment, the fluorescence signal associated with the coacervates flowed inward immediately and dispersed rapidly throughout the cytoplasm (26 min) (Fig. 5b). This observation eliminated the possibility of coacervate entry via simple membrane pores or ruptures.

Macropinocytosis is characterized by intense actin polymerization that drives the formation of large membrane folds and indentations, ultimately generating macropinosomes.[96–98] Shebanova and Miserez et al. elucidated that HBpep-SP coacervates with a zeta potential of approximately +5.9 mV and an average size of 1 μm enter Hela-GFP cells through a process combining features of macropinocytosis and phagocytosis, involving active cytoskeletal remodelling and filopodia-like protrusions from filopodia capture, early engulfment, late engulfment to internalization (Fig. 5c).[99] Inhibitor assays using SMIFH2 (formin-inhibitor), CK666 (Arp2/3-inhibitor), and nocodazole (tube-inhibitor), revealed that formin-mediated linear actin polymerization constituted the core driving pathway, while Arp2/3-regulated branched actin networks provided auxiliary enhancement, and microtubules contributed
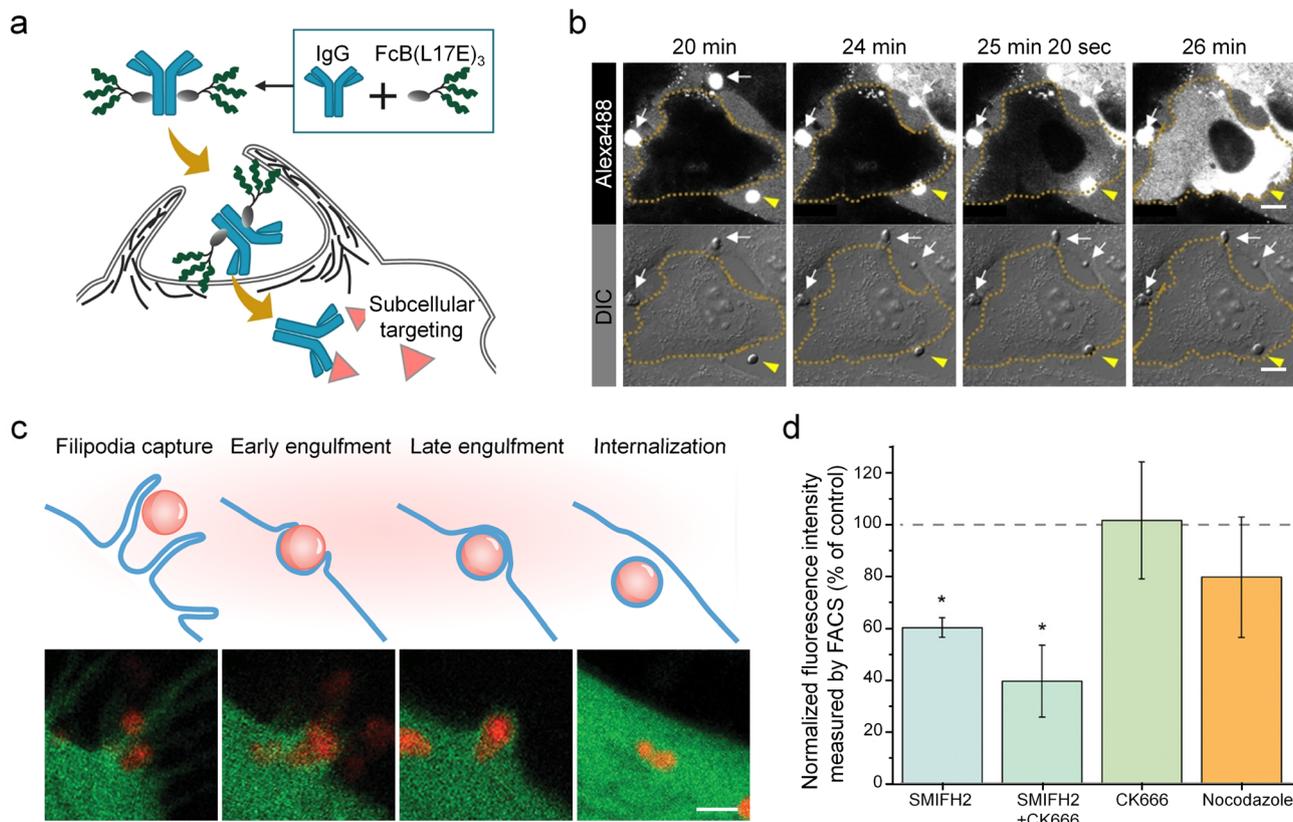
Fig. 5 Actin polymerization-mediated endocytosis of coacervates by phospholipid membranes. (a) Schematic diagram showing IgG intracellular delivery *via* the Fc-binding L17E trimer conjugate [FcB(L17E)$_3$]. (b) Time-lapse microscopy images presenting the sedimentation, membrane contact, and subsequent intracellular distribution of Alexa488-IgG. Arrows indicate the initial sedimentation of particle-like IgG structures (white) and their eventual contact with the cell membrane, leading to signal influx into the cell (yellow arrow; cell boundary outline by dashed line). (c) Schematic diagrams and fluorescence microscopy images showing the uptake process of mCherry coacervates by HeLa-GFP cells, from filipodia capture, early engulfment, late engulfment to internalization. (d) FACS analysis of mCherry-loaded HB*pep*-SP coacervate uptake by HeLa-GFP cells in the presence of SMIFH2 (formin-inhibitor), CK666 (Arp2/3-inhibitor), and nocodazole (tube-inhibitor), revealing that formin-mediated linear actin polymerization constituted the core driving pathway, while Arp2/3-regulated branched actin networks provided auxiliary enhancement. Scale bars: 10 μm (b) and 2 μm (c). (a and b) Reproduced with permission from ref. 95. Copyright (2021) Wiley-VCH. (c and d) Reproduced with permission from ref. 99. Copyright (2024) Wiley-VCH.

through transport functions (Fig. 5d). These processes were regulated by signalling hubs such as Rac1 and Cdc42,[100] deepening the understanding of coacervate-based intracellular delivery strategies and pathways underlying macropinocytosis in cellular adaptation and nutrient acquisition. Currently, work on actin polymerization focuses on establishing quantitative structure–function relationships between actin remodelling efficiency and coacervate composition, with particular emphasis on minimizing off-target cytoskeletal effects. Additionally, the development of single-particle tracking methodologies capable of resolving both actin dynamics and coacervate movement simultaneously remains a key technological challenge.

4. Coacervates crossing phospholipid membranes by direct penetration

Direct penetration represents a crucial transmembrane mechanism through which coacervates traverse lipid bilayers without

vesicle formation. This section introduces two principal pathways underlying this mechanism. The first involves lipid raft-mediated translocation, in which coacervates utilize ordered lipid raft domains to achieve direct membrane penetration. The second mechanism is membrane defect-facilitated passage, whereby coacervates traverse the bilayer through structural imperfections and localized lipid extraction.

4.1 Penetration mediated by lipid rafts

Evidence indicated that certain coacervates entered cells *via* a passive, lipid raft-dependent endocytosis.[101] Sun and Miserez *et al.* mentioned that the cellular uptake of short His-rich, pH-responsive beak peptide (HB*pep*) coacervates was prevented by methyl-β-cyclodextrin (MβCD, depleting cholesterol in the membrane through dissolution) and low temperature (4 °C, reducing membrane fluidity), suggesting a passive and potentially cholesterol-dependent pathway bypassing classical endocytosis.[102] HB*pep*-SR (the sole Lys residue with a self-immolative moiety) underwent coacervation under near-neutral pH

conditions, efficiently recruiting macromolecular therapeutics within the resulting coacervates. Upon incubation with cells, these cargo-loaded coacervates traversed the cell membrane *via* a cholesterol-dependent, lipid raft-mediated direct cytosolic delivery. Following internalization into the cytosol, the coacervates were reduced by glutathione, triggering their disassembly and the subsequent release of the therapeutic payload (Fig. 6a). Hoechst and LysoTracker staining revealed no co-localization with HepG2 cell nucleus and acidic organelles such as lysosomes, confirming that HB*pep*-SP (conjugated peptides with phenyl groups, eGFP-loaded) coacervates avoided endosomal capture (Fig. 6b). Furthermore, coacervate internalization remained unaffected by several canonical endocytic inhibitors

targeting energy metabolism (sodium azide, NaN$_3$), macropinocytosis (amiloride, AM), and clathrin-mediated endocytosis (chlorpromazine, CPZ) with two control groups included: untreated cells (negative control, NC) and cells treated with eGFP-loaded coacervates without inhibitors (blank) confirming that this pathway was distinct from classical, actively regulated endocytosis (Fig. 6c). By utilizing lipid raft-mediated pathways, these coacervates achieved efficient cellular entry while bypassing endosomal sequestration, enabling direct cytoplasmic delivery of cargoes including proteins, peptides and mRNA. Notably, the same research group reported that these HB*pep*-SP coacervates entering HepG2 cells also involved an actin polymerization-driven vesicular engulfment pathway. This
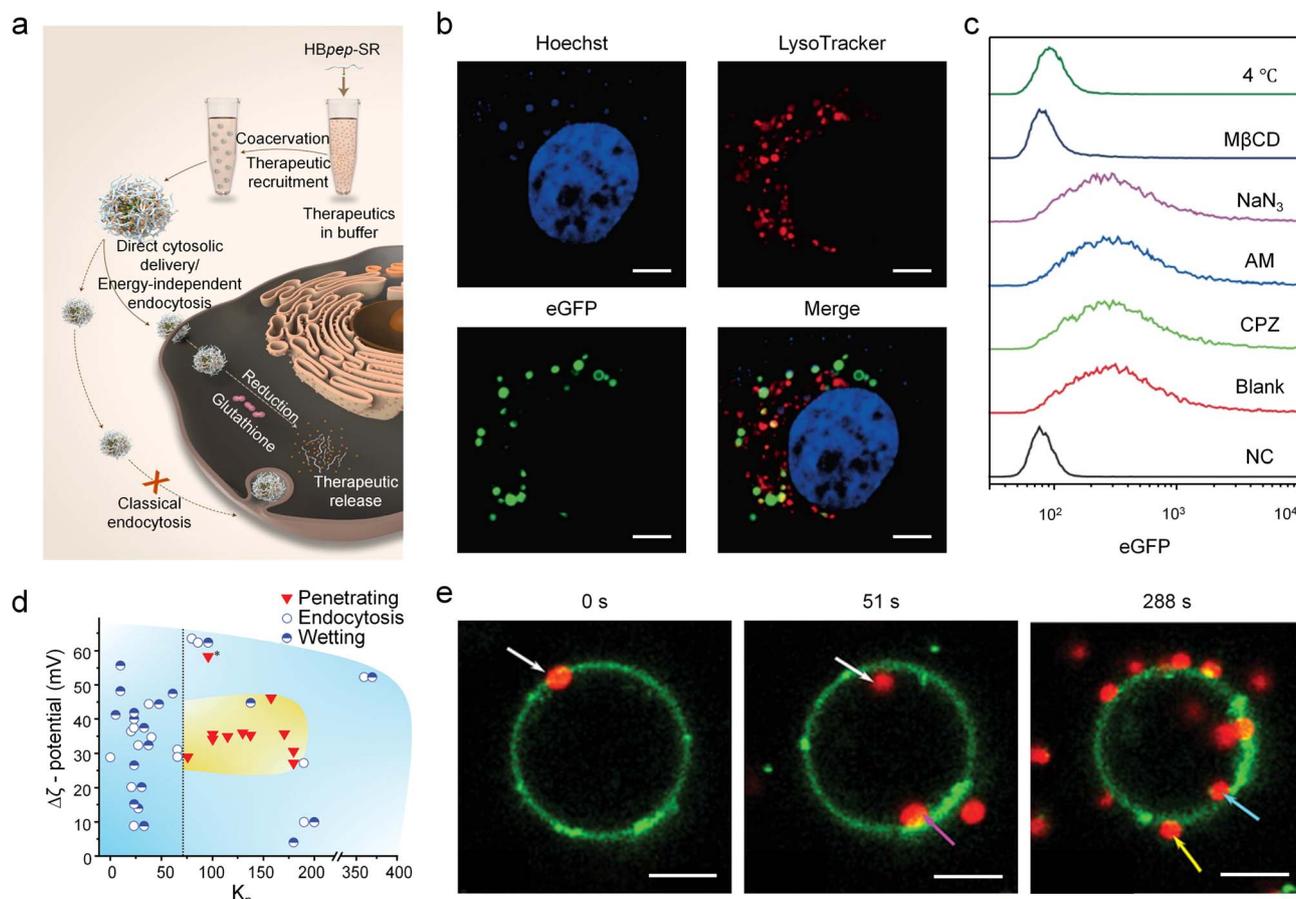

Fig. 6 Lipid raft- and phospholipid defect-mediated direct penetration of coacervates across phospholipid membranes. (a) Schematic diagram of redox-responsive peptide coacervates HB*pep*-SR entering cells *via* lipid raft-mediated endocytosis bypassing the clathrin-mediated classical endocytosis. (b) Fluorescence microscopy images showing that coacervates (green) did not co-localize with lysosomes (red). (c) FACS analysis of HepG2 cells untreated/treated with various inhibitors indicated that only cholesterol-depleting compounds (MβCD) and low temperature of 4 °C showed inhibition of cellular uptake. Inhibitors that prevented energy metabolism (NaN$_3$), macropinocytosis (AM), and clathrin-mediated endocytosis (CPZ) did not show inhibition of cellular uptake. Totally untreated cells (NC) and cells treated by eGFP-loaded coacervates without any inhibitors (blank) were included as control. (d) Morphological state diagram of coacervate–liposome interactions as a function of Δζ (absolute ζ-potential difference) and K_p (coacervate lipid partition coefficient). Different interaction states are denoted by red inverted triangles (penetration), open circles (endocytosis), and half-filled circles (wetting). Penetration was observed exclusively in the region (yellow-shaded area) defined by K_p values above 75 (right of the black dashed line) and a Δζ between 25 and 45 mV, and never occurred at K_p values below ≈75 (left of the black dashed line). An exception marked with an asterisk (*) was observed for R$_{40}$/polyA coacervates (average diameter <1 μm), which penetrated liposomes despite strong surface attraction. (e) Time-lapse CLSM images showing penetration of R$_{10}$/tyRNA coacervates (red) into a liposome (green). The liposome diameter decreased by 3.8 μm between 0 s and 288 s, suggesting the uptake of phospholipids from liposomes by coacervates. Scale bars: 10 μm (b) and 10 μm (e). (a–c) Reproduced with permission from ref. 102. Copyright (2022) Springer Nature. (d and e) Reproduced with permission from ref. 103. Copyright (2023) Wiley-VCH.

suggests that multiple transmembrane pathways may coexist for identical coacervate–cell pairs, or that more advanced characterization is needed to fully resolve the process under these conditions.

4.2 Penetration mediated by phospholipid defects

Direct penetration governed by the physicochemical properties of coacervates involves the active extraction of phospholipids and the consequent generation of transient pores. Evidences demonstrated that coacervates assembled from arginine-rich oligomers and oligonucleotides incorporated lipid molecules during membrane interaction, perturbing the local membrane architecture and facilitating the formation of transient permeation pathways. The process was framed within a quantitative morphological state diagram where coacervate–liposome interactions were classified by two key parameters involving the absolute zeta-potential difference and the coacervate lipid partition coefficient (Fig. 6d).[103] Penetration (triangles) occurred exclusively when the partition coefficient exceeded 75 and the zeta-potential difference was between 25 and 45 mV. This parameter space supported sufficient lipid uptake alongside a moderate electrostatic driving force. Endocytosis (open circles) and wetting (half-filled circles) generally occurred outside the yellow-shaded region, particularly when the partition coefficient fell below approximately 75. An exception was noted for sub-micrometre R_{40}/polyA coacervates, which achieved penetration despite high surface attraction, indicating that coacervate size also influenced direct membrane transit.[103] The dynamic of phospholipid extraction was further visualized by time-lapse confocal laser scanning microscopy (CLSM) imaging of R_{10}/tyRNA coacervates (red) penetrating liposomes (green). A 3.8 µm reduction in liposome diameter observed between 0 s and 288 s confirmed that coacervates absorbed phospholipids from the membrane during penetration (Fig. 6e). The formation of transient pores was further supported by membrane permeability assays. Upon interaction with R_{10}-FAM/(ACTG)$_2$ coacervates, a time-dependent increase in fluorescence intensity was observed inside liposomes, indicating diffusion of fluorescent molecules from the external solution into the liposomes. Together, these findings demonstrated a direct-penetration pathway in which coacervates remodelled the membrane by lipid acquisition, thereby enabling traversal into the interior of cells or liposomes.

Furthermore, coacervates exhibited direct membrane penetration capabilities analogous to those of cell-penetrating peptides, polymers, and nanoparticles. Although the traditional view held that only small-sized particles (e.g., nanoparticles) directly penetrated cell membranes, recent studies have confirmed that certain coacervates also possessed this capability. Jin and Jeong et al. established a direct membrane penetration pathway for intrinsically disordered protein-inspired nanovector-based coacervates (IDP-NCs), which entirely bypassed endocytosis.[104] Their uptake remained highly efficient (>80%) even after treatment with a comprehensive panel of endocytosis inhibitors targeting clathrin-, caveolae/lipid raft-, energy-, and receptor-mediated pathways. Similarly,

coacervates composed of cationic peptides and polymers with similar compositions to cell-penetrating peptides also demonstrated the ability to directly penetrate the cell membrane.[103] This direct penetration was achieved through interactions with molecules on the cell membrane surface, which altered the local membrane properties and enabled the coacervates to pass through. Nevertheless, the molecular mechanism underlying the direct penetration of cell membranes by coacervates remains unclear and requires further investigation to elucidate its detailed processes and principles.

5. Conclusion and perspective

To summarize, achieving a systematic understanding of coacervate transmembrane mechanisms is essential for enabling the rational design of synthetic cells, biosensors and drug-delivery systems. This review classifies them into vesicular engulfment driven by electrostatic interaction, photoswitchable phospholipids, caveolin, or actin polymerization and direct penetration mediated by lipid rafts or phospholipid defects. They are governed by fluidity and charge of coacervates and liposomes or cells, and the size ratio between coacervates and liposomes and cells, which collectively determine the energetic balance between adhesion and internalization. Furthermore, for identical coacervate–cell systems, multiple transmembrane pathways may coexist, underscoring the need for further characterization and investigation to fully resolve the underlying pathways.

Despite significant progress, several critical challenges remain underexplored. First, the real-time dynamics and detailed mechanism underlying coacervate–phospholipid membrane interaction remain unclear owing to a lack of direct experimental observation. During internalization, key intermediate events such as transient pore formation, lipid extraction, and local membrane curvature changes and potential structural reorganization of the coacervates themselves, cannot be tracked with nanoscale spatial and millisecond temporal resolution. Advancing this area depends on the development of in situ, real-time super-resolution characterization techniques including minimal fluorescence photon flux microscopy (MINFLUX), stimulated emission depletion microscopy (STED), and instant structured illumination microscopy (iSIM). Second, the design of coacervates as transmembrane delivery carriers still lacks predictability and accurate anticipation of membrane responses or uptake pathways. In particular, how composition-dependent parameters (e.g., charge density, hydrophobicity, and molecular weight of coacervate component) regulate lipid interactions, membrane remodelling, and cargo release kinetics remains poorly understood. Thus, more detailed studies integrating artificial intelligence to build quantitative models that link coacervate parameters (e.g., composition, charge, and size) to membrane responses are needed, enabling the rational design of specific transmembrane pathways and guiding coacervates from passive recognition to active selection. Finally, coacervate–phospholipid membrane interactions rely primarily on passive, nonspecific electrostatic interaction, which lacks target specificity and spatiotemporal control preventing

directed communication and precise transmembrane delivery. To overcome this, a programmable interaction-regulatory system can be developed to integrate responsive molecular switches (*e.g.*, light and magnetic fields), target modules (*e.g.*, nucleic acid aptamers and specific antibodies), and microenvironment-sensors (*e.g.*, pH-responsive lipids and enzyme-cleavable peptide sequences). This programmable approach would facilitate directed signalling and dynamic information exchange between artificial cells and natural cells, laying a technical foundation for next-generation targeted delivery and intelligent diagnostics and therapeutics platforms.

Author contributions

Y. Q. led and supervised the project. H. Y. prepared the original draft. H. Y., M. W. and Y. Q. revised the manuscript.

Conflicts of interest

The authors declare that they have no conflicts of interest.

Data availability

Data availability is not applicable to this article, as no new data were generated or analyzed as part of this review.

Acknowledgements

References

1 A. Honigmann and A. Pralle, Compartmentalization of the cell membrane, *J. Mol. Biol.*, 2016, **428**(24), 4739–4748.

2 E. Gouaux and R. MacKinnon, Principles of selective ion transport in channels and pumps, *Science*, 2005, **310**(5753), 1461–1465.

3 W. Stillwell, in *An introduction to biological membranes*, ed. W. Stillwell, Elsevier, 2013, ch. 14, pp. 305–337.

4 E. Tekle, R. D. Astumian and P. B. Chock, Selective and asymmetric molecular transport across electroporated cell membranes, *Proc. Natl. Acad. Sci. U. S. A.*, 1994, **91**(24), 11512–11516.

5 X. Cheng and J. C. Smith, Biological membrane organization and cellular signaling, *Chem. Rev.*, 2019, **119**(9), 5849–5880.

6 D. Casares, P. V. Escribá and C. A. Rosselló, Membrane lipid composition: Effect on membrane and organelle structure, function and compartmentalization and therapeutic avenues, *Int. J. Mol. Sci.*, 2019, **20**, 2167.

7 K. Simons and D. Toomre, Lipid rafts and signal transduction, *Nat. Rev. Mol. Cell Biol.*, 2000, **1**(1), 31–39.

8 P. Mitchell, The protonmotive Q cycle: A general formulation, *FEBS Lett.*, 1975, **59**(2), 137–139.

9 A. Ben-Shem, F. Frolow and N. Nelson, Crystal structure of plant photosystem I, *Nature*, 2003, **426**(6967), 630–635.

10 J. T. Davis, O. Okunola and R. Quesada, Recent advances in the transmembrane transport of anions, *Chem. Soc. Rev.*, 2010, **39**(10), 3843–3862.

11 C. Miller, Clc chloride channels viewed through a transporter lens, *Nature*, 2006, **440**(7083), 484–489.

12 L. Chen, W. Si, L. Zhang, G. Tang, Z.-T. Li and J.-L. Hou, Chiral selective transmembrane transport of amino acids through artificial channels, *J. Am. Chem. Soc.*, 2013, **135**(6), 2152–2155.

13 K. Sawada, N. Echigo, N. Juge, T. Miyaji, M. Otsuka, H. Omote, A. Yamamoto and Y. Moriyama, Identification of a vesicular nucleotide transporter, *Proc. Natl. Acad. Sci. U. S. A.*, 2008, **105**(15), 5683–5686.

14 S. Gallegos, C. Pacheco, C. Peters, C. M. Opazo and L. G. Aguayo, Features of alpha-synuclein that could explain the progression and irreversibility of parkinson's disease, *Front. Neurosci.*, 2015, **9**, 59.

15 C. Palm-Apergi, P. Lönn and S. F. Dowdy, Do cell-penetrating peptides actually "penetrate" cellular membranes?, *Mol. Ther.*, 2012, **20**(4), 695–697.

16 O. D. Murillo, W. Thistlethwaite, J. Rozowsky, S. L. Subramanian, R. Lucero, N. Shah, A. R. Jackson, S. Srinivasan, A. Chung, C. D. Laurent, R. R. Kitchen, T. Galeev, J. Warrell, J. A. Diao, J. A. Welsh, K. Hanspers, A. Riutta, S. Burgstaller-Muehlbacher, R. V. Shah, A. Yeri, L. M. Jenkins, M. E. Ahsen, C. Cordon-Cardo, N. Dogra, S. M. Gifford, J. T. Smith, G. Stolovitzky, A. K. Tewari, B. H. Wunsch, K. K. Yadav, K. M. Danielson, J. Filant, C. Moeller, P. Nejad, A. Paul, B. Simonson, D. K. Wong, X. Zhang, L. Balaj, R. Gandhi, A. K. Sood, R. P. Alexander, L. Wang, C. Wu, D. T. W. Wong, D. J. Galas, K. V. Keuren-Jensen, T. C. Patel, J. C. Jones, S. Das, K.-H. Cheung, A. R. Pico, A. I. Su, R. L. Raffai, L. C. Laurent, M. E. Roth, M. B. Gerstein and A. Milosavljević, exRNA atlas analysis reveals distinct extracellular RNA cargo types and their carriers present across human biofluids, *Cell*, 2019, **177**(2), 463–477.

17 J. K. Leypoldt and L. W. Henderson, Molecular charge influences transperitoneal macromolecule transport, *Kidney Int.*, 1993, **43**(4), 837–844.

18 D. M. Pegtel and S. J. Gould, Exosomes, *Annu. Rev. Biochem.*, 2019, **88**, 487–514.

19 S. Nagata, Apoptosis and clearance of apoptotic cells, *Annu. Rev. Immunol.*, 2018, **36**, 489–517.

20 T. Stylianopoulos, M.-Z. Poh, N. Insin, M. G. Bawendi, D. Fukumura, L. L. Munn and R. K. Jain, Diffusion of particles in the extracellular matrix: The effect of repulsive electrostatic interactions, *Biophys. J.*, 2010, **99**(5), 1342–1349.

21 M. Kaksonen and A. Roux, Mechanisms of clathrin-mediated endocytosis, *Nat. Rev. Mol. Cell Biol.*, 2018, **19**(5), 313–326.

22 D. Barman and R. Drolia, Caveolin-mediated endocytosis: Bacterial pathogen exploitation and host–pathogen interaction, *Cells*, 2025, **14**, 2.

23 N. J. Yang and M. J. Hinner, Getting across the cell membrane: An overview for small molecules, peptides, and proteins, *Site-specific protein labeling: Methods and protocols*, 2015, pp. 29–53.

24 J. A. Swanson and C. Watts, Macropinocytosis, *Trends Cell Biol.*, 1995, **5**(11), 424–428.

25 C. Contini, From light to life-like protocells, *Nat. Synth.*, 2025, **4**(11), 1329–1330.

26 J. v. d. Gucht, E. Spruijt, M. Lemmers and M. A. C. Cohen Stuart, Polyelectrolyte complexes: Bulk phases and colloidal systems, *J. Colloid Interface Sci.*, 2011, **361**(2), 407–422.

27 S. L. Perry, Phase separation: Bridging polymer physics and biology, *Curr. Opin. Colloid Interface Sci.*, 2019, **39**, 86–97.

28 S. Zhou, X. Ju, H. Chen, Y. Zhang, J. Zheng, K. Wang, X. Yang and J. Liu, Light-responsive DNA droplets for controlling enzyme cascade pathways by dynamic phase separation, *Angew. Chem., Int. Ed.*, 2025, **64**(31), e202505316.

29 M. Lee, S. L. Perry and R. C. Hayward, Complex coacervation of polymerized ionic liquids in non-aqueous solvents, *ACS Polym. Au*, 2021, **1**(2), 100–106.

30 Y. Huang, J. Huang, W. Yin, F. Xie, B. Coleman, Y. Cao, S. Aya, W. Zhu, Z. Yang and L. Jiang, Encoding coacervate droplets with paramagnetism for dynamical reconfigurability and spatial addressability, *ACS Nano*, 2023, **17**(7), 6234–6246.

31 F. Li, Y. Lin and Y. Qiao, Regulating FUS liquid-liquid phase separation *via* specific metal recognition, *Chin. J. Polym. Sci.*, 2022, **40**(9), 1043–1049.

32 T. Z. Jia, K. Chandru, Y. Hongo, R. Afrin, T. Usui, K. Myojo and H. J. Cleaves, Membraneless polyester microdroplets as primordial compartments at the origins of life, *Proc. Natl. Acad. Sci. U. S. A.*, 2019, **116**(32), 15830–15835.

33 L. Jia, Z. Ji, Y.-m. Ji, C. Zhou, G.-w. Xing and Y. Qiao, Design and fluorescence localization of lipid-rich domains in multiphase coacervate droplets based on aie-active molecules, *ChemSystemsChem*, 2021, **3**(2), e2000044.

34 S. Ye, A. P. Latham, Y. Tang, C.-H. Hsiung, J. Chen, F. Luo, Y. Liu, B. Zhang and X. Zhang, Micropolarity governs the structural organization of biomolecular condensates, *Nat. Chem. Biol.*, 2024, **20**(4), 443–451.

35 Z. Liu, Y. Ji, W. Mu, X. Liu, L. Y. Huang, T. Ding and Y. Qiao, Coacervate microdroplets incorporating J-aggregates toward photoactive membraneless protocells, *Chem. Commun.*, 2022, **58**(15), 2536–2539.

36 Y. Ji, W. Mu, H. Wu and Y. Qiao, Directing transition of synthetic protocell models *via* physicochemical cues-triggered interfacial dynamic covalent chemistry, *Adv. Sci.*, 2021, **8**(18), 2101187.

37 Y. Zhang, Y. Chen, X. Yang, X. He, M. Li, S. Liu, K. Wang, J. Liu and S. Mann, Giant coacervate vesicles as an integrated approach to cytomimetic modeling, *J. Am. Chem. Soc.*, 2021, **143**(7), 2866–2874.

38 W. Mu, Z. Ji, M. Zhou, J. Wu, Y. Lin and Y. Qiao, Membrane-confined liquid-liquid phase separation toward artificial organelles, *Sci. Adv.*, 2021, **7**(22), eabf9000.

39 X. Hao, J. Li, B. Zhang, X. Zhang, X. Liu, H. Shi and H. Yang, Transforming crowded coacervates into multi-compartmental hybrid microreactors for practical enzymatic catalysis, *Angew. Chem., Int. Ed.*, 2025, **64**(43), e202502479.

40 Y. Yin, H. Chang, H. Jing, Z. Zhang, D. Yan, S. Mann and D. Liang, Electric field-induced circulation and vacuolization regulate enzyme reactions in coacervate-based protocells, *Soft Matter*, 2018, **14**(31), 6514–6520.

41 D. Wang, L. Zhou, X. Zhang, Z. Zhou, Z. Huang and N. Gao, Supramolecular switching of liquid-liquid phase separation for orchestrating enzyme kinetics, *Angew. Chem., Int. Ed.*, 2025, **64**(14), e202422601.

42 Y. Qiao, M. Li, D. Qiu and S. Mann, Response-retaliation behavior in synthetic protocell communities, *Angew. Chem., Int. Ed.*, 2019, **58**(49), 17758–17763.

43 H. Chen, W. Xu, H. Shi, Y. Qiao, X. He, J. Zheng, S. Zhou, X. Yang, K. Wang and J. Liu, DNA-based artificial receptors as transmembrane signal transduction systems for protocellular communication, *Angew. Chem., Int. Ed.*, 2023, **62**(23), e202301559.

44 A. Samanta, V. Sabatino, T. R. Ward and A. Walther, Functional and morphological adaptation in DNA protocells *via* signal processing prompted by artificial metalloenzymes, *Nat. Nanotechnol.*, 2020, **15**(11), 914–921.

45 T. Mashima, M. H. M. E. v. Stevendaal, F. R. A. Cornelissens, A. F. Mason, B. J. H. M. Rosier, W. J. Altenburg, K. Oohora, S. Hirayama, T. Hayashi, J. C. M. v. Hest and L. Brunsveld, DNA-mediated protein shuttling between coacervate-based artificial cells, *Angew. Chem., Int. Ed.*, 2022, **61**(17), e202115041.

46 Y. Ji, Y. Lin and Y. Qiao, Plant cell-inspired membranization of coacervate protocells with a structured polysaccharide layer, *J. Am. Chem. Soc.*, 2023, **145**(23), 12576–12585.

47 Q.-H. Zhao, F.-H. Cao, Z.-H. Luo, W. T. S. Huck and N.-N. Deng, Photoswitchable molecular communication between programmable DNA-based artificial membraneless organelles, *Angew. Chem., Int. Ed.*, 2022, **61**(14), e202117500.

48 Y. Qiao, M. Li, R. Booth and S. Mann, Predatory behaviour in synthetic protocell communities, *Nat. Chem.*, 2017, **9**(2), 110–119.

49 N. Gao, C. Xu, Z. Yin, M. Li and S. Mann, Triggerable protocell capture in nanoparticle-caged coacervate microdroplets, *J. Am. Chem. Soc.*, 2022, **144**(9), 3855–3862.

50 A. Boija, I. A. Klein, B. R. Sabari, A. Dall'Agnese, E. L. Coffey, A. V. Zamudio, C. H. Li, K. Shrinivas, J. C. Manteiga, N. M. Hannett, B. J. Abraham, L. K. Afeyan, Y. E. Guo, J. K. Rimel, C. B. Fant, J. Schuijers, T. I. Lee, D. J. Taatjes and R. A. Young, Transcription factors activate genes

through the phase-separation capacity of their activation domains, *Cell*, 2018, **175**(7), 1842–1855.

51 W. Shao, X. Bi, Y. Pan, B. Gao, J. Wu, Y. Yin, Z. Liu, M. Peng, W. Zhang, X. Jiang, W. Ren, Y. Xu, Z. Wu, K. Wang, G. Zhan, J. Y. Lu, X. Han, T. Li, J. Wang, G. Li, H. Deng, B. Li and X. Shen, Phase separation of RNA-binding protein promotes polymerase binding and transcription, *Nat. Chem. Biol.*, 2022, **18**(1), 70–80.

52 V. H. Ryan, G. L. Dignon, G. H. Zerze, C. V. Chabata, R. Silva, A. E. Conicella, J. Amaya, K. A. Burke, J. Mittal and N. L. Fawzi, Mechanistic view of hnRNPA2 low-complexity domain structure, interactions, and phase separation altered by mutation and arginine methylation, *Mol. Cell*, 2018, **69**(3), 465–479.

53 S. Kilic, A. Lezaja, M. Gatti, E. Bianco, J. Michelena, R. Imhof and M. Altmeyer, Phase separation of 53BP1 determines liquid-like behavior of DNA repair compartments, *EMBO J.*, 2019, **38**(16), EMBJ2018101379.

54 Y. Yang, T. L. Willis, R. W. Button, C. J. Strang, Y. Fu, X. Wen, P. R. C. Grayson, T. Evans, R. J. Sipthorpe, S. L. Roberts, B. Hu, J. Zhang, B. Lu and S. Luo, Cytoplasmic DAXX drives SQSTM1/p62 phase condensation to activate Nrf2-mediated stress response, *Nat. Commun.*, 2019, **10**(1), 3759.

55 M. Du and Z. J. Chen, DNA-induced liquid phase condensation of cgas activates innate immune signaling, *Science*, 2018, **361**(6403), 704–709.

56 C. P. Brangwynne, T. J. Mitchison and A. A. Hyman, Active liquid-like behavior of nucleoli determines their size and shape in xenopus laevis oocytes, *Proc. Natl. Acad. Sci. U. S. A.*, 2011, **108**(11), 4334–4339.

57 P. M. Favi, S. Yi, S. C. Lenaghan, L. Xia and M. Zhang, Inspiration from the natural world: From bio-adhesives to bio-inspired adhesives, *J. Adhes. Sci. Technol.*, 2014, **28**(3–4), 290–319.

58 Q. Guo, G. Zou, X. Qian, S. Chen, H. Gao and J. Yu, Hydrogen-bonds mediate liquid-liquid phase separation of mussel derived adhesive peptides, *Nat. Commun.*, 2022, **13**(1), 5771.

59 B. K. Ahn, S. Das, R. Linstadt, Y. Kaufman, N. R. Martinez-Rodriguez, R. Mirshafian, E. Kesselman, Y. Talmon, B. H. Lipshutz, J. N. Israelachvili and J. H. Waite, High-performance mussel-inspired adhesives of reduced complexity, *Nat. Commun.*, 2015, **6**(1), 8663.

60 J. Liu, L. Tian, Y. Qiao, S. Zhou, A. J. Patil, K. Wang, M. Li and S. Mann, Hydrogel-immobilized coacervate droplets as modular microreactor assemblies, *Angew. Chem., Int. Ed.*, 2020, **59**(17), 6634.

61 N. R. Johnson and Y. Wang, Coacervate delivery systems for proteins and small molecule drugs, *Expert Opin. Drug Delivery*, 2014, **11**(12), 1829–1832.

62 K. O. Margossian, M. U. Brown, T. Emrick and M. Muthukumar, Coacervation in polyzwitterion-polyelectrolyte systems and their potential applications for gastrointestinal drug delivery platforms, *Nat. Commun.*, 2022, **13**(1), 2250.

63 I. Santiago and F. C. Simmel, Self-propulsion strategies for artificial cell-like compartments, *Nanomaterials*, 2019, **9**, 1680.

64 J. Ouyang, J. Chen, Z. Wu, K. You, T. Chen, Y. Q. Gao, P. Li, X. Zhang and T. Li, Navigating condensate micropolarity to enhance small-molecule drug targeting, *Nat. Chem. Biol.*, 2025, **22**, 593–603.

65 J. Wang, M. Abbas, Y. Huang, J. Wang and Y. Li, Redox-responsive peptide-based complex coacervates as delivery vehicles with controlled release of proteinous drugs, *Commun. Chem.*, 2023, **6**(1), 243.

66 C. Wang, J. You, M. Gao, P. Zhang, G. Xu and H. Dou, Bio-inspired gene carriers with low cytotoxicity constructed *via* the assembly of dextran nanogels and nano-coacervates, *Nanomedicine*, 2020, **15**(13), 1285–1296.

67 S. S. Nasr, S. Lee, D. Thiyagarajan, A. Boese, B. Loretz and C.-M. Lehr, Co-delivery of mRNA and pDNA using thermally stabilized coacervate-based core-shell nanosystems, *Pharmaceutics*, 2021, **13**, 1924.

68 Y. Huang, H. Chen, X. Qiao, S. Li, X. Wang, X. Liu and X. Huang, Liquid-liquid phase separation-boosted transmembrane delivery in interactive protocell communities, *Nat. Commun.*, 2025, **16**(1), 5231.

69 E. Spruijt, J. Sprakel, M. A. Cohen Stuart and J. v. d. Gucht, Interfacial tension between a complex coacervate phase and its coexisting aqueous phase, *Soft Matter*, 2010, **6**(1), 172–178.

70 J. Guzowski, P. M. Korczyk, S. Jakiela and P. Garstecki, The structure and stability of multiple micro-droplets, *Soft Matter*, 2012, **8**(27), 7269–7278.

71 U. Seifert, K. Berndl and R. Lipowsky, Shape transformations of vesicles: Phase diagram for spontaneous-curvature and bilayer-coupling models, *Phys. Rev. A*, 1991, **44**(2), 1182–1202.

72 M. M. Anila, R. Ghosh and B. Różycki, Membrane curvature sensing by model biomolecular condensates, *Soft Matter*, 2023, **19**(20), 3723–3732.

73 V. Satarifard and R. Lipowsky, Mutual remodeling of interacting nanodroplets and vesicles, *Commun. Phys.*, 2023, **6**(1), 6.

74 R. Ghosh, V. Satarifard and R. Lipowsky, Different pathways for engulfment and endocytosis of liquid droplets by nanovesicles, *Nat. Commun.*, 2023, **14**(1), 615.

75 H.-F. Renard and E. Boucrot, Unconventional endocytic mechanisms, *Curr. Opin. Cell Biol.*, 2021, **71**, 120–129.

76 G. J. Doherty and H. T. McMahon, Mechanisms of endocytosis, *Annu. Rev. Biochem.*, 2009, **78**(1), 857–902.

77 K. G. Rothberg, J. E. Heuser, W. C. Donzell, Y.-S. Ying, J. R. Glenney and R. G. W. Anderson, Caveolin, a protein component of caveolae membrane coats, *Cell*, 1992, **68**(4), 673–682.

78 T. Lu, S. Liese, L. Schoenmakers, C. A. Weber, H. Suzuki, W. T. S. Huck and E. Spruijt, Endocytosis of coacervates into liposomes, *J. Am. Chem. Soc.*, 2022, **144**(30), 13451–13455.

79 A. Mangiarotti, N. Chen, Z. Zhao, R. Lipowsky and R. Dimova, Wetting and complex remodeling of

membranes by biomolecular condensates, *Nat. Commun.*, 2023, **14**(1), 2809.

80 J. P. K. Armstrong, S. N. Olof, M. D. Jakimowicz, A. P. Hollander, S. Mann, S. A. Davis, M. J. Miles, A. J. Patil and A. W. Perriman, Cell paintballing using optically targeted coacervate microdroplets, *Chem. Sci.*, 2015, **6**(11), 6106–6111.

81 J. Käs and E. Sackmann, Shape transitions and shape stability of giant phospholipid vesicles in pure water induced by area-to-volume changes, *Biophys. J.*, 1991, **60**(4), 825–844.

82 R. Dimova, K. A. Riske, S. Aranda, N. Bezlyepkina, R. L. Knorr and R. Lipowsky, Giant vesicles in electric fields, *Soft Matter*, 2007, **3**(7), 817–827.

83 R. Dimova and K. A. Riske, Electrodeformation, electroporation, and electrofusion of giant unilamellar vesicles, *Handbook of Electroporation*, 2017, pp. 235–252.

84 S. Aranda, K. A. Riske, R. Lipowsky and R. Dimova, Morphological transitions of vesicles induced by alternating electric fields, *Biophys. J.*, 2008, **95**(2), L19–L21.

85 N. Khalifat, N. Puff, S. Bonneau, J.-B. Fournier and M. I. Angelova, Membrane deformation under local pH gradient: Mimicking mitochondrial cristae dynamics, *Biophys. J.*, 2008, **95**(10), 4924–4933.

86 R. Lipowsky, Understanding membranes and vesicles: A personal recollection of the last two decades, *Phys. Biol. Membr.*, 2018, 3–44.

87 R. Lipowsky and R. Dimova, Introduction to remodeling of biomembranes, *Soft Matter*, 2021, **17**(2), 214–221.

88 S. H. Yun and S. J. J. Kwok, Light in diagnosis, therapy and surgery, *Nat. Biomed. Eng.*, 2017, **1**(1), 0008.

89 A. Mangiarotti, M. Aleksanyan, M. Siri, T.-W. Sun, R. Lipowsky and R. Dimova, Photoswitchable endocytosis of biomolecular condensates in giant vesicles, *Adv. Sci.*, 2024, **11**(23), 2309864.

90 G. W. Gould and J. Lippincott-Schwartz, New roles for endosomes: From vesicular carriers to multi-purpose platforms, *Nat. Rev. Mol. Cell Biol.*, 2009, **10**(4), 287–292.

91 M. Halder, Z. Jin, K. Li, L. Amer, T. He, S. Han, X. Zhong, N. K. Devaraj and J. V. Jokerst, β-sheet structures enhance aggregation-induced emission signals in peptide-based coacervates, *Chem. Mater.*, 2025, **37**(19), 7588–7602.

92 A. E. Carlsson, Membrane bending by actin polymerization, *Curr. Opin. Cell Biol.*, 2018, **50**, 1–7.

93 P. Lappalainen, T. Kotila, A. Jégou and G. Romet-Lemonne, Biochemical and mechanical regulation of actin dynamics, *Nat. Rev. Mol. Cell Biol.*, 2022, **23**(12), 836–852.

94 Y. Kawaguchi, A. Kikkawa, S. Kimura, H. Abe and S. Futaki, Microcondensate-mediated intracellular infusion of mRNA

across the plasma membrane, *Angew. Chem., Int. Ed.*, 2026, **65**(1), e12139.

95 T. Iwata, H. Hirose, K. Sakamoto, Y. Hirai, J. V. V. Arafiles, M. Akishiba, M. Imanishi and S. Futaki, Liquid droplet formation and facile cytosolic translocation of IgG in the presence of attenuated cationic amphiphilic lytic peptides, *Angew. Chem., Int. Ed.*, 2021, **60**(36), 19804–19812.

96 B. J. Li, B. K C, T. Nii, T. Mori, Y. Katayama and A. Kishimura, Designable synthetic complex coacervates enabling protein delivery to cells, *Polym. J.*, 2025, **57**(8), 911–922.

97 Y. Bao, Z. Xu, K. Cheng, X. Li, F. Chen, D. Yuan, F. Zhang, A. R.-Y. Che, X. Zeng, Y.-D. Zhao and J. Xia, Staudinger reaction-responsive coacervates for cytosolic antibody delivery and TRIM21-mediated protein degradation, *J. Am. Chem. Soc.*, 2025, **147**(4), 3830–3839.

98 Y. Bao and J. Xia, Phase-separated coacervates of low-molecular-weight compounds for cytosolic delivery and disease treatment, *JACS Au*, 2025, **5**(11), 5267–5285.

99 A. Shebanova, Q. M. Perrin, K. Zhu, S. Gudlur, Z. Chen, Y. Sun, C. Huang, Z. W. Lim, E. A. Mondarte, R. Sun, S. Lim, J. Yu, Y. Miao, A. N. Parikh, A. Ludwig and A. Miserez, Cellular uptake of phase-separating peptide coacervates, *Adv. Sci.*, 2024, **11**(42), 2402652.

100 N. Lamarche, N. Tapon, L. Stowers, P. D. Burbelo, P. Aspenström, T. Bridges, J. Chant and A. Hall, Rac and Cdc42 induce actin polymerization and G1 cell cycle progression independently of p65PAK and the JNK/SAPK MAP kinase cascade, *Cell*, 1996, **87**(3), 519–529.

101 S. Ren, X. Lin, Q. Xie, S. Yu, X. Zheng, H. Pan, S. Tan, Y. Wang, S. Zhang, T. Li, S. Ge, J. Zhang and N. Xia, Redox-responsive peptide coacervates for enhanced mRNA delivery and intracellular release, *ACS Nano*, 2026, **20**(1), 459–474.

102 Y. Sun, S. Y. Lau, Z. W. Lim, S. C. Chang, F. Ghadessy, A. Partridge and A. Miserez, Phase-separating peptides for direct cytosolic delivery and redox-activated release of macromolecular therapeutics, *Nat. Chem.*, 2022, **14**(3), 274–283.

103 T. Lu, X. Hu, M. H. I. v. Haren, E. Spruijt and W. T. S. Huck, Structure-property relationships governing membrane-penetrating behaviour of complex coacervates, *Small*, 2023, **19**(38), 2303138.

104 S. Jin, H. Park, S. M. Ryu, D. Guk, J. Lee, S. Jin, C. Keum, J. Park, M. H. Park, C. Kim, H. Kim, J. Noh, K. H. Lee, J. H. Ryu and Y. Jeong, Intrinsically disordered protein-inspired nanovector-based coacervates for the direct cytosolic transport of biomacromolecules, *Adv. Mater.*, 2025, e07877.